Histogram method to obtain heat capacities in lipid monolayers, curved bilayers, and membranes containing peptides

Vesselka P. Ivanova and Thomas Heimburg*
Membrane Thermodynamics Group, Max-Planck-Institute for Biophysical Chemistry, D-37077 Göttingen, Germany
(Received 1 June 2000; revised manuscript received 10 November 2000; published 29 March 2001)

Lipid monolayer chain melting transitions were simulated using a two-state Doniach model, and experimental melting profiles of lipid vesicles were analyzed. We sampled the information of a Monte Carlo simulation into a single broad histogram containing complete information about the distribution of states. The information of the monolayer histogram was first used to calculate the melting behavior of a bilayer constructed from two uncoupled monolayers. We then fitted calorimetric heat profiles of various preparations of dipalmitoyl phosphatidylcholine vesicles. This analysis was extended to lipid bilayers. A fixed mean bilayer curvature was shown to result in a broadening of bilayer melting profiles. We furthermore used the histogram method to obtain the chain melting behavior of simple lipid-peptide mixtures.

DOI: 10.1103/PhysRevE.63.041914 PACS number(s): 87.16.Ac, 87.16.Dg, 87.15.Kg, 64.60.Cn

I. INTRODUCTION

Many biological membrane lipids melt in a physiologically relevant temperature regime. They undergo a chain-order transition from a gel phase to a fluid phase, which has been treated extensively in the literature. Besides the use of mean-field theories for describing lipid melting [1–5], which approximate some fluctuating features of the membrane system into average quantities, a common approach consists of the application of statistical thermodynamics models that describe the local nature of the fluctuations more accurately [6]. These models usually reduce the wealth of states of individual lipids into subensembles with given average energies and entropies. Ising-like two state models with only gel and fluid lipid states (also called Doniach models) have been shown to describe transitions adequately [7–11] (see also the recent review in Ref. [12]), but models employing more states have also been used, such as the ten-state Pink model [13,6,14]. Ising and Pink models were compared by Mouritsen *et al.* [3], and found to yield comparable results outside of a first-order transition regime. The distribution of states was then explored with Monte Carlo simulations. The advantage of such statistical thermodynamics treatments over mean-field approaches is that they provide insight into the magnitude of enthalpy or volume fluctuations [15], and into domain formation [16,17] within the lipid membrane plane. The obvious disadvantage is that the Monte Carlo–like simulations used to evaluate the models produce no analytical solutions and are partially time consuming. The main motivation for employing Monte Carlo simulations is that in complex systems the degeneracy of the microconfigurations of the ensemble does not have an analytical solution, and thus has to be explored numerically. Ferrenberg and Swendsen [18] pointed out in 1988 that the information from Monte Carlo simulations can be used in a much more efficient way if the degeneracy of microstates of previous simulations is not recalculated for each set of parameters. Since this degeneracy is independent of the parameters (such as melting energies or interactions energies) of the system, it can be mapped into histograms consisting of small bins covering the phase space. Once the degeneracy of microstates is known, it can be used to generate solutions for general sets of parameters in the proximity of the previous parameter set. This solution is then quasianalytical. This concept has been widely used to reduce computer time, for example to describe transitions in two-dimensional systems. In lipid systems it has been used for Ising-like (Doniach) models [19] or Pink models [20–22]. One problem with this kind of analysis is that usually in Monte Carlo simulations only a small part of the phase space is explored, which limits the applicability of the Ferrenberg-Swendsen approach. For some simple systems, however, it is possible to collect information about the degeneracy of states for the entire (accessible) phase space, either by performing Monte Carlo simulations close to critical points where fluctuations are very high [19], or by combining histograms of simulations using various parameter sets [23]. For the two-state Ising model this is quite simple, since it has only two variables—the number of spins in either state and the number of nearest neighbor interactions of unlike spins. For such a system the phase space can be rastered into two-dimensional histograms, where the information about the states in a small volume of the phase space is collected into bins.

With few exceptions [20,11], the melting of lipid membranes has been modeled with monolayer simulations. This implicitly requires that a bilayer system consists of uncoupled monolayers. In experimental systems, however, vesicles are usually not freely fluctuating membrane sheets but are rather located in vesicular systems of predefined geometry; the fluctuations in the two monolayers are usually not uncoupled [11]. Lipids change their area by about 25% upon melting. An asymmetry of the areas of the two monolayers automatically induces a bilayer curvature. If the curvature is fixed, the fluctuations in area on both monolayers are confined such that on average the area difference on both

*Email address: theimbu@gwdg.de, WWW: www.gwdg.de/ theimbu

monolayers is constant. This results in a coupling of the fluctuations in both monolayers.

The curvature elasticity of membranes is coupled to the lateral monolayer compressibility [24]. The monolayer compressibility, however, is a function of the area fluctuations, which are also related to the heat capacity [15,25]. Since curvature constrains the area fluctuations it must have an influence on the heat capacity [26]. Experimentally it has been found that supported membranes with fixed curvature display broadened c_P profiles [27].

In this paper we describe transitions in lipid systems with a broad histogram technique for monolayer systems, based on a Doniach model. The term ''broad histogram'' stands for a histogram that covers information about the entire phase space, usually obtained by a combination of many histograms that were obtained with various sets of simulation parameters (e.g., at different temperatures or for different values of the melting enthalpy). We extended the method to describe bilayer systems consisting of two coupled monolayers. From this we derived heat capacity profiles of bilayers in confined flat or curved geometries. Furthermore, we used this method to describe the heat capacity profiles of a membrane containing peptides that resemble either the gel or the fluid lipid state.

II. MATERIALS AND METHODS

Dipalmitoyl phosphatidylcholine was purchased from Avanti Polar Lipids (Birmingham, AL), and used without further purification. Vesicles were prepared in a buffer [2–5-mM Hepes (4-(2-hydroxyethyl)-1-piperazineethanesulfonic acid) EDTA (ethylenedinitrillo tetraacetic acid), *p*H 7.5] with lipid concentrations of about 10 mM. Multilamellar vesicles (MLV's) form spontaneously by dispersing the lipids in buffer and gentle shaking above the melting temperature of 41.5 °C. Small unilamellar vesicles (SUV's) were prepared by ultrasonication with 50 W for several minutes using a Model W185 sonifier from Heat System-Ultrasonics (Plainview, NY). Since SUV's are unstable below the melting temperature, the respective calorimetric scans were performed in the down scan mode. Gradually small vesicles spontaneously fuse into large unilamellar vesicles (LUV's). To prepare LUV's, SUV's were stored in a refrigerator at 4 °C for about two weeks.

Vesicle sizes for the different preparations have been determined using a ''Nicomp 370 Autodilute Submicron Particle Sizer'' (Pacific Scientific, Menlo Park, CA). The diameter of the SUV was determined to be about 25 ± 5 nm, the diameter of the LUV was 140 ± 10 nm, and the diameter of the MLV was about 1.5 ± 0.2 μm.

Calorimetric experiments were performed on a VP calorimeter by Microcal (Northampton, MA). Calorimetric scans were performed at scan rates of 5°/h (LUV and SUV) and 0.3°/h (MLV).

Monte Carlo simulations were performed on triangular 31×31 and 101×101 lattices with periodic boundaries using a Glauber algorithm as described in Refs. [8,10]. For a typical histogram for a single set of parameters 10^6 Monte Carlo cycles were performed, taking about 30 mins on a LINUX-based 600-MHz PC with a Pentium III processor. One Monte Carlo cycle corresponds to one attempt on average to change the state of each matrix site. For the broad histogram to cover the relevant parts of the phase space, about 100 single histograms were matched. Each histogram contained 100×200 bins.

III. THEORY AND RESULTS

A. Monolayers

In previous publications [8,10,19,11] it was shown that a two-dimensional Ising model is well suited for describing the chain melting transition of lipid membranes. This kind of description is sometimes referred to as the Doniach model [7]. Two lipid states are distributed on a triangular lattice, representing an ordered gel state and an unordered fluid state of the individual lipids. For historical reasons, instead of attributing two different spin values, we denote the two states with index g (gel) and index f (fluid)

The Hamiltonian of such a system can be written as

$$\mathcal{H}=n_gE_g+n_fE_f+n_{gg}\epsilon_{gg}+n_{gf}\epsilon_{gf}+n_{ff}\epsilon_{ff}, \qquad (3.1)$$

where E_g and E_f are the internal energies of gel and fluid states, and ϵ_{gg}, ϵ_{gf}, and ϵ_{ff} are the nearest neighbor contact energies between two gel lipids, a gel and a fluid lipid, and two fluid lipids, respectively. The numbers n_g and n_f are the numbers of gel and fluid molecules in a given matrix, whereas n_{gg}, n_{gf}, and n_{ff} represent the numbers of respective nearest neighbor contacts.

Sugar *et al.* [8] pointed out that this can be rewritten to yield

$$\mathcal{H}=nE_0+n_f\Delta E+n_{gf}\omega_{gf},$$

$$E_0=E_g+\frac{z}{2}\epsilon_{gg},$$

$$\Delta E=\left(E_f+\frac{z}{2}\epsilon_{ff}\right)-\left(E_g+\frac{z}{2}\epsilon_{gg}\right), \qquad (3.2)$$

$$\omega_{gf}=\epsilon_{gf}-\frac{\epsilon_{gg}+\epsilon_{gf}}{2},$$

with a coordination number $z=6$ for a triangular lattice. We formally can assign volumes and areas to each lipid state (at each site) [7]. Doniach modified his model such that each spin represents a given area A_g or A_f, and we can also introduce the volumes of each site, V_g or V_f. We therefore define the enthalpy of a microconfiguration

$$H=nH_0+n_f\Delta H+n_{gf}\omega_{gf}$$

$$H_0=E_0+pV_g+\Pi A_g,$$

$$\Delta H(n_f,n_{gf})=\Delta E+p\Delta V+\Pi\Delta A, \qquad (3.3)$$

$$\Delta V=V_f-V_g,$$

$$\Delta A=A_f-A_g,$$

introducing a bulk pressure p and a lateral pressure Π.

The two lipid states are defined to be degenerate with entropies, S_g and S_f [7]. The free energy difference of each microstate with respect to the ground state (all lipids are gel lipids with $E=E_0$) is given by

$$\Delta G(n_f,n_{gf})=n_f(\Delta H-T\Delta S)+n_{gf}\omega_{gf} \tag{3.4}$$

$$\Delta S=S_f-S_g,$$

The model described in Eqs. (3.4) resembles an Ising model in a field, where $(\Delta H-T\Delta S)$ acts as the temperature dependent field. For each set of variables n_f and n_{gf}, there may be various possible lipid arrangements on the matrix. Thus each membrane state is degenerate. When the simulation is compared to a calorimetric experiment, the enthalpy difference ΔH corresponds to the calorimetric heat of melting, integrated over all temperatures. ΔH therefore does not reflect a latent heat (which would depend on simulation parameters), but is a parameter independent number that can directly be taken from a calorimetric experiment. The entropy difference ΔS reflects the different order of the lipid chains in the gel and the fluid state. It can also be determined from calorimetry using the relation $\Delta S=\Delta H/T_m$, where T_m is the melting temperature. At T_m the field $(\Delta H-T\Delta S)$ is zero, and both lipid states are equally probable. The interaction parameter ω_{gf} determines the cooperativity (or the transition halfwidth) of the melting process. The phase space (variables n_f and n_{gf}) can be explored in Monte Carlo simulations [8,10].

The mean value $\langle X\rangle$ of any physical observable can be obtained by averaging over all bilayer configurations at a particular temperature T, using the statistical thermodynamics expression

$$\langle X(n_f,n_{gf},\zeta)\rangle=\sum_{n_f}\sum_{n_{gf}}X(n_f,n_{gf},\zeta)P(n_f,n_{gf},\zeta), \tag{3.5}$$

with the partition coefficients

$$P(n_f,n_{gf},\zeta)=\frac{\Omega(n_f,n_{gf})\exp\left(-\dfrac{\Delta G(n_f,n_{gf},\zeta)}{RT}\right)}{\displaystyle\sum_{n_f}\sum_{n_{gf}}\Omega(n_f,n_{gf})\exp\left(-\frac{\Delta G(n_f,n_{gf},\zeta)}{RT}\right)}, \tag{3.6}$$

where ζ denotes the set of parameters, $[\Delta H,\Delta S,\omega_{gf},T]$. $P(n_f,n_{gf},\zeta)$ is the probability to find a bilayer configuration, with n_f lipids being in the fluid state and n_{gf} gel-fluid contacts [7]. $\Omega(n_f,n_{gf})$ is the number of microstates with given n_f and n_{gf}, i.e., the density of states. It does not depend on the parameters ζ of the simulation, but depends only on the matrix size of the simulation. Thus, once determined, it can be used to calculate the mean value of an observable $\langle X\rangle$ for any given set of values for the parameters,ζ, by using Eqs. (3.5) and (3.6) [18]. $\langle X\rangle$ may represent the enthalpy $\langle H\rangle$ the mean square of the enthalpy, $\langle H^2\rangle$, the mean volume $\langle V\rangle$, and the mean monolayer area $\langle A\rangle$. These mean values can be used to calculate the heat capacity,

$$c_p=\frac{\langle H^2\rangle-\langle H\rangle^2}{RT^2}, \tag{3.7}$$

the isothermal volume compressibility,

$$\kappa_T^{vol}=\frac{\langle V^2\rangle-\langle V\rangle^2}{\langle V\rangle RT} \tag{3.8}$$

or the isothermal area compressibility,

$$\kappa_T^{area}=\frac{\langle A^2\rangle-\langle A\rangle^2}{\langle A\rangle RT}, \tag{3.9}$$

Each Monte Carlo (MC) simulation produces a distribution of states $P(n_f,n_{gf},\zeta)$ which can be sampled into bins containing the sum of the probabilities in a segment of phase space. The distribution of states in the two-dimensional model of a lipid monolayer depends on two variables, n_f and n_{gf}. In our simulations, the information about the probability distribution is put into a two-dimensional histogram with 100×200 bins. The histogram may be used to determine the probability distribution at any other set of parameters ζ^* [18]:

$$P^*(n_f,n_{gf},\zeta^*)=\frac{P(n_f,n_{gf},\zeta)\exp\left(\dfrac{\Delta G(n_f,n_{gf},\zeta)}{RT}-\dfrac{\Delta G^*(n_f,n_{gf},\zeta^*)}{RT^*}\right)}{\displaystyle\sum_{n_f}\sum_{n_{gf}}P(n_f,n_{gf},\zeta)\exp\left(\frac{\Delta G(n_f,n_{gf},\zeta)}{RT}-\frac{\Delta G^*(n_f,n_{gf},\zeta^*)}{RT^*}\right)} \tag{3.10}$$

It is evident that the probability distribution $P^*(n_f,n_{gf},\zeta^*)$ can only be used to calculate thermodynamic functions if the distribution $P(n_f,n_{gf},\zeta)$ covers most of the available phase space. Because of finite Monte Carlo sampling, it is not possible to cover the whole configuration space (n_f,n_{gf}) by a single histogram. Figure 1 shows a representative histogram for a monolayer for a continuous transition (no latent heat) at the heat capacity maximum. The statistics of MC sampling is good close to the distribution maximum. It is bad, however, in the outer wings of the distribution. Thus the size of the

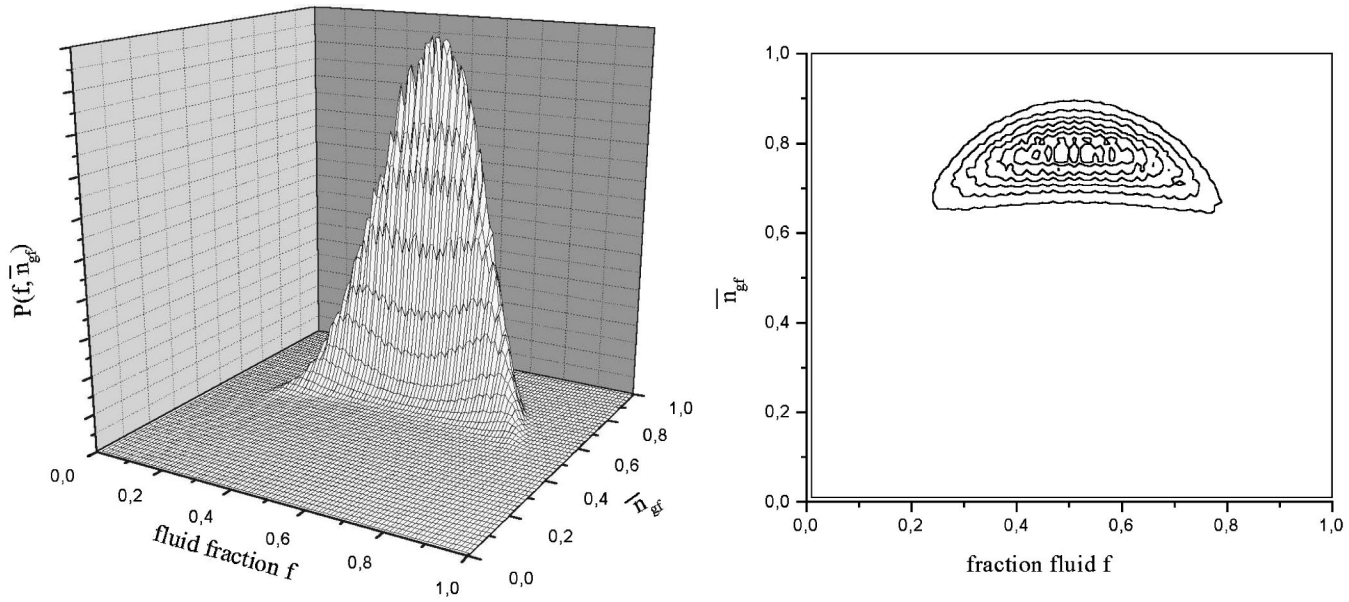

FIG. 1. Histogram of the distribution of states of a monolayer at the melting temperature T_m for $\omega_{gf}=1.3$ kJ/mol (continuous transition).

original histogram limits the range where Eq. (3.10) is applicable. The accuracy of this procedure, however, can be significantly improved when histograms obtained for various sets of parameters ζ^* are merged into one large histogram [23,28]. This is done in the following manner: In the region where the primary histogram overlaps with a secondary distribution, the secondary histogram is recalculated with Eq. (3.10) using the parameter set ζ of the primary histogram. In the wings of the distribution, where Monte Carlo sampling is bad, it was replaced by a secondary distribution using an equivalent volume method as outlined in Ref. [28]. The concept of equivalent volumes yields a scaling ratio, which was used for subsequent merging of the two histograms into one. This matching method is very similar to the ''multistage sampling'' technique of Valleau and Card [29], who considered overlapping energy distributions in the calculation of the free energy of the system of hard spheres with Coulombic forces.

The combination of many histograms into one is shown in Fig. 2 (left hand panel) for 12 histograms (obtained for a fixed value for w_{gf} at different temperatures), and for 84 histograms (obtained for a general set of different temperatures T and cooperativity parameters w_{gf}) in Fig. 2 (right hand panel). The outer limits of the histograms, where the statistics are on the verge of being significant, are shown. The latter broad histogram covers all the relevant phase

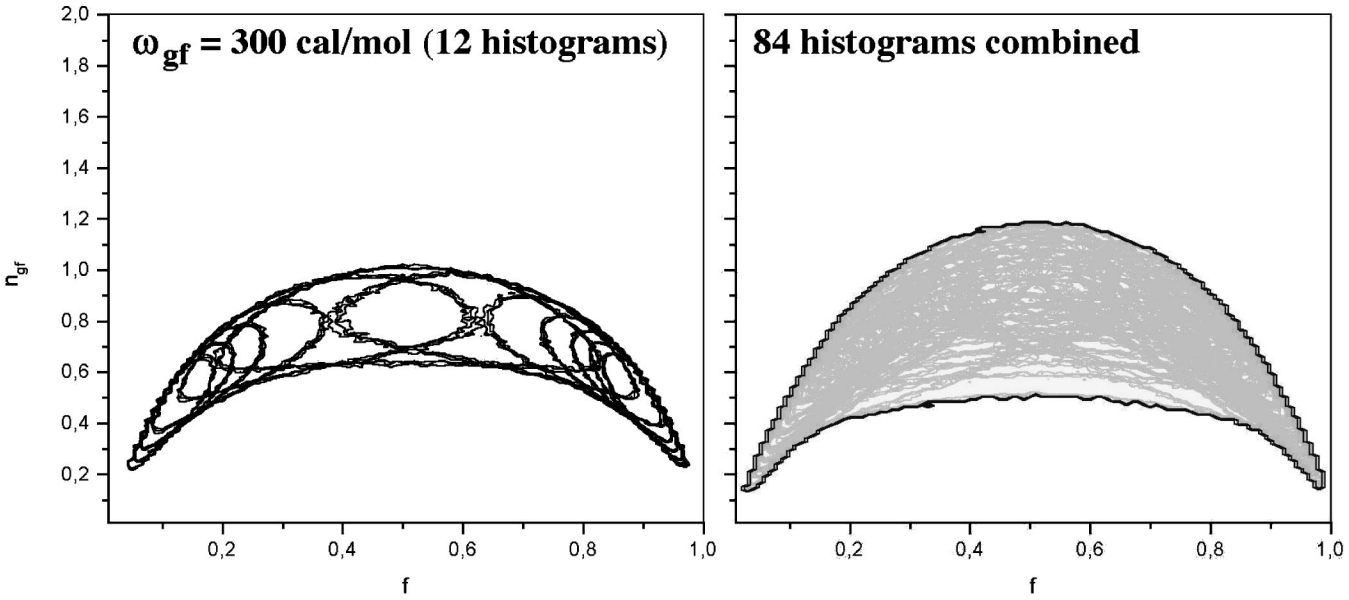

FIG. 2. Matching of histograms obtained for different sets of parameters. The large histogram, shown on the right side, covers the relevant range of the phase sphase.

space necessary to describe lipid transitions.

From this general histogram the individual histograms for a fixed set of parameters ζ can be obtained. In Fig. 3 (left hand panel) the effect of temperature changes close to the melting point (fixed w_{gf}) on the histograms is shown. The distribution maximum moves to larger values of n_f with increasing temperature, because lipids are melting. The right hand panel shows histograms obtained at the heat capacity maximum with different values for the cooperativity parameter w_{gf}. Upon an increase in w_{gf}, the histogram undergoes a change from a profile with a Gaussian cross-section to a histogram with two maxima. While the first histogram indicates that the transition is continuous, the latter corresponds to a first-order behavior where two membrane states may coexist. The middle panel of Fig. 3(b) shows a monolayer close to its critical point. Note that the half width of the maxima in the histogram is finite. This is due to the finite size of the computer matrix. To summarize this we conclude that we are able to collect the information about the phase space such that histograms for each set of parameters can be obtained without performing additional Monte Carlo simulations. Thus we are able to quasianalytically generate heat capacity profiles for each set of parameters, $(\Delta H, \Delta S, w_{gf})$.

Let us assume that a lipid bilayer consists of two uncoupled monolayers (meaning that each monolayer may explore the phase space without any correlation with the other monolayer). Under these conditions the histogram technique can be used to generate quasianalytical fits for experimentally obtained heat capacity profiles (Fig. 4). The three parameters entering Eq. (3.10) (ΔH, ΔS, and w_{gf}) can be determined from the integrated heat capacity, the melting point, and the transition halfwidth. In Fig. 4 this has been done for three different preparations of dipalmitoyl phosphatidylcholine (DPPC) vesicles. When dispersed in water, DPPC spontaneously forms MLV's in a size range of up to 1000 nm (Fig. 4, left). These vesicles can be transformed into SUV's of approximately 25-nm radius by ultrasonification (Fig. 4, right), as judged from light scattering. These vesicles are metastable and slowly fuse into LUV's of a diameter of approximately 140 nm (Fig. 4, center). It can immediately be seen that the three vesicle preparations display very different transition cooperativities. MLV's display a transition halfwidth of less than 0.1°, whereas LUV's show a 1° halfwidth and SUV's a 2°–3° halfwidth. The second peak in the SUV preparation stems from LUV formed by some spontaneous fusion events (cf. center trace). Also shown in Fig. 4 are fits to the curves using the histogram technique. The input parameters into the calculation are the experimental values for the melting enthalpy, ΔH, and the melting entropy, $\Delta S = \Delta H / T_m$. Disregarding the different shapes of the three transitions, the enthalpies used for fitting were the same ($\Delta H = 36$ kJ/mol). To obtain calculated profiles similar to the experimental curves, we mainly adjusted the cooperativity parameter, w_{gf}. For MLV's we used $w_{gf} = 1578$ J/mol, for LUV's 1245 J/mol and for the SUV's 1138 J/mol. It can be seen that unlike nearest neighbor contributions are relatively small (about 0.5 kT per interaction), and that relatively small changes in this parameter may significantly influence the shape of the heat capacity profiles. Also, the value for MLV's corresponds to a first-order-like transition (cf. Fig. 3) whereas the values for LUV's and SUV's rather correspond to a continuous transition. This supports the general notion that lipid melting transitions are generally close to the critical point. It should be noted at this point that the exact number of w_{gf} for MLV's (first-order case) should not be taken too seriously since it depends on finite size effects. To demonstrate this we performed a finite size scaling analysis (shown as insets in Fig. 4), comparing the results from the histograms obtained from simulations on a 31×31 matrix to those obtained from simulations on a 101×101 matrix. The matrix size has no influence on the calculated heat capacity profiles of LUV's and SUV's. This is different for MLV's. Using the same value for ω_{gf} as for the 31×31 matrix, the heat capacity anomaly obtained from a 101×101 matrix became too narrow be detected in our simulations. In fact, the exact shape of the experimental heat capacity profiles of MLV's cannot be described by the Ising model using large matrices with any set of parameters. Possibly domains in multilayers are finite. When analyzing the MLV data with an all-or-nothing transition with a fixed cooperative unit size of 750 lipids [10] (which is close to the 31×31 matrix size) we obtained good agreement with the experimental data (cf. Ref. [10]). This may be due to the fact that multilamellar membranes in the gel phase are structured into a periodical ripple pattern, which was recently postulated to define an upper limit to the domain size [11]. It also cannot be excluded that due to the very narrow transition halfwidth of MLV dispersions ($\leqslant 0.1°$) inhomogeneities in the size distribution play a role.

B. Bilayers

The lipid bilayer is composed of two monolayers with partition functions Q_{M_1} and Q_{M_2}. If the two monolayers are uncoupled ($Q_{M_1} = Q_{M_2}$), the partition function of the bilayer, Q_B, is the product of the monolayer partition functions,

$$Q_B = Q_{M_1} Q_{M_2} = \sum_{n_f^1} \sum_{n_{gf}^1} \sum_{n_f^2} \sum_{n_{gf}^2} P_B(n_f^1, n_{gf}^1, n_f^2, n_{gf}^2, \zeta), \tag{3.11}$$

with a set of parameters $\zeta = [\Delta H, \Delta S, \omega_{gf}, T]$ and the bilayer partition coefficients

$$P_B(n_f^1, n_{gf}^1, n_f^2, n_{gf}^2, \zeta) = P_{M_1}(n_f^1, n_{gf}^1, \zeta) P_{M_2}(n_f^2, n_{gf}^2, \zeta). \tag{3.12}$$

In a recent publication [15], we argued that the Ising model may be well suited to describe not only enthalpy changes in transition regimes, but also the volume and area changes. We based our argument on the experimental finding that enthalpy and volume changes are proportional functions of temperature, and, further, that bending elasticities predicted from heat capacity profiles are very close to experimental values [15,30]. For this reason we assume in the following that each individual lipid in the matrix possesses two states of enthalpy, entropy, volume, and area, respectively. The volume difference of the two lipid states is defined by

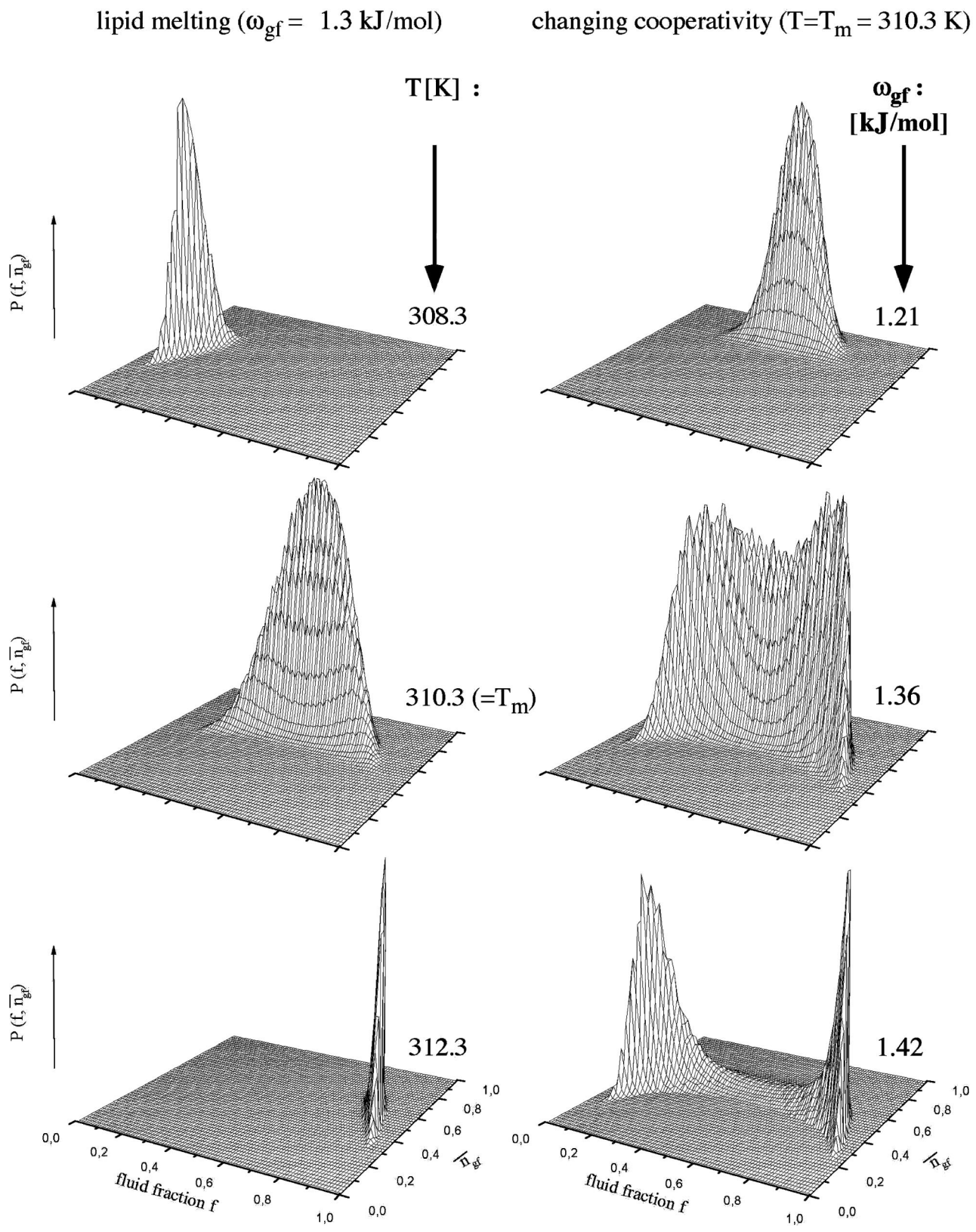

FIG. 3. Histograms of the distribution of states of a monolayer. Left: At different temperatures for $\omega_{gf}=1.245$ kJ/mol below T_m, at T_m and above T_m. Right: For different cooperativities ($\omega_{gf}=1.21$, 1.36, and 1.42 kJ/mol at the melting temperature T_m. The top histogram represents a continuous transition, the center histogram corresponds to a situation close to the critical point, and the bottom histogram shows a first-order-like behavior. Note the finite size effects. The histogram was obtained from a Monte Carlo simulation performed on a 31 $\times$31 matrix.

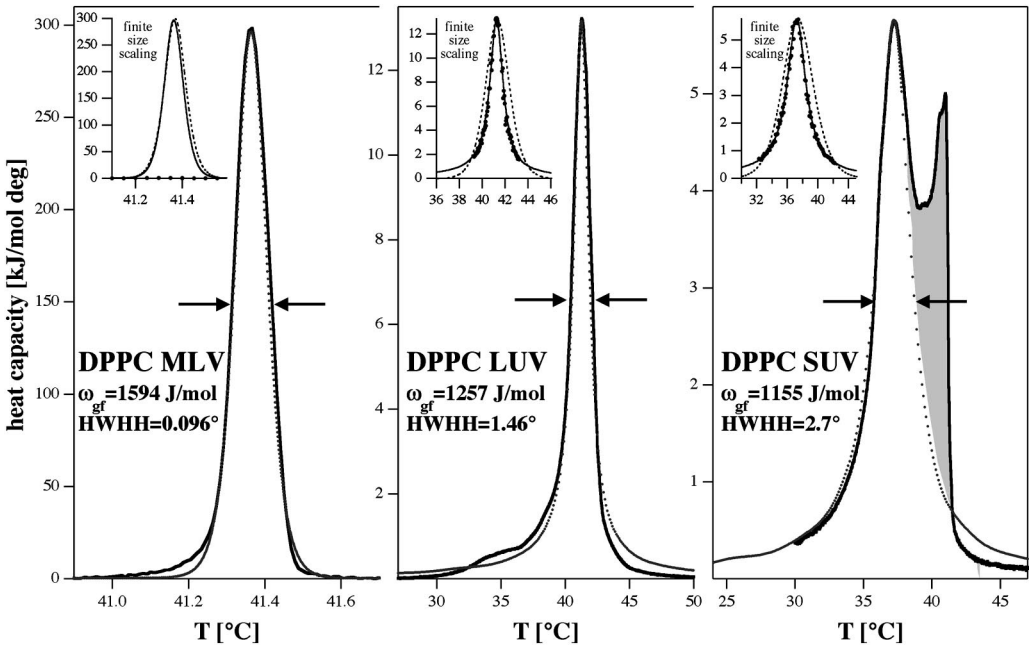

FIG. 4. Fits of experimental heat capacity profiles of dipalmitoyl phosphatidylcholine (DPPC) vesicles from different preparations, using the histogram method. Dotted grey lines indicate the fits, solid black lines the experimental results. Left: multilamellar vesicles (MLV's); center: large unilamellar vesicles (LUV's); right: small unilamellar vesicles (SUV's). The shaded area represents a residual fraction of LUV's in the SUV preparation. Note the different scaling of the temperature axes. The MLV transition is very cooperative with a halfwidth of less than 0.1°. Fitting parameters are given in the text. The histogram was constructed on the basis of a 31×31 matrix. Insets: finite size scaling analysis; solid lines are the fits from the 31×31 matrix simulation, and closed circles were obtained from a 101×101 matrix simulation using identical parameters. The dotted lines correspond to an all-or-nothing transition with a fixed cooperative unit size of 750 for MLV's, 33 for LUV's and 16.5 for SUV's. For LUV's and SUV's the fits did not depend on matrix size. An all-or-nothing transition did not yield a reasonable description of the experimental profiles. For MLV's, no fit with our model using large matrices could be obtained. However, an all-or-nothing transition with a finite cooperative unit size of 750 lipids describes the experimental results very well.

$\Delta V=V_f-V_g$, and the area difference by $\Delta A=A_f-A_g$ (where A_f and A_g are the areas of fluid and gel lipids, respectively). For simplicity we furthermore assume that the coordination number of the lipids in the matrix is unaffected by area changes. According to Eq. (3.5), the temperature dependence of the mean monolayer area can be calculated.

In a bilayer, independent area fluctuations of both monolayers only occur if the monolayers are uncoupled. If the two monolayers M_1 and M_2 have different areas, then the bilayer will be curved. Let us assume that the area difference can be used to calculate a mean radius of curvature r or a mean curvature $c=1/r$, as shown schematically in Fig. 5,

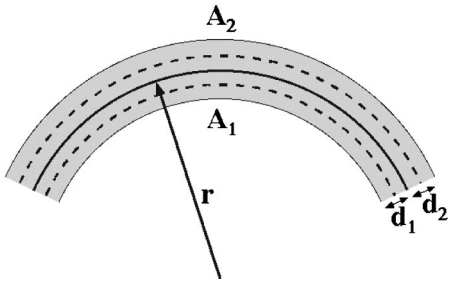

FIG. 5. Schematic representation of a curved bilayer, indicating area and thickness of the two monolayers.

$$r=\frac{1}{c}=\frac{1}{2}\,\frac{\sqrt{A_1}d_2+\sqrt{A_2}d_1}{\sqrt{A_2}-\sqrt{A_1}} \tag{3.13}$$

where A_1 and A_2 are the total areas of monolayers 1 and 2 in the center of each monolayer segment with n lipids, constructed as the sum of all individual lipid areas by $A_{1,2}=nA_g+n_f^{1,2}\Delta A$. The monolayer thickness, defined as the average lipid length, is given by $d_{1,2}=1/n(nd_g+n_f^{1,2}\Delta d)$. The curvature c is a function of the number of fluid lipids, n_f^1 and n_f^2, on either side. This coupling of membrane curvature to monolayer areas was first proposed in Ref. [24]. Values for ΔA and Δd were taken from the literature [15]. In our picture we assume that area changes close to a transition are dominated by the melting process of the membrane. We neglect area changes due to fluctuations of individual molecules other than those caused by chain isomerizations. In an unconstrained bilayer the mean curvature is a fluctuating property.

Real membranes, however, are usually not freely fluctuating systems [11]. They exist in MLV's which are constrained to a macroscopically nearly flat surface by adjacent layers. Large or small vesicles are closed structures with a given mean curvature. A similar situation can be found in supported membranes (Fig. 6). If the curvature $c_0=1/r_0$ is fixed, the curvature fluctuations of the bilayer are inhibited.

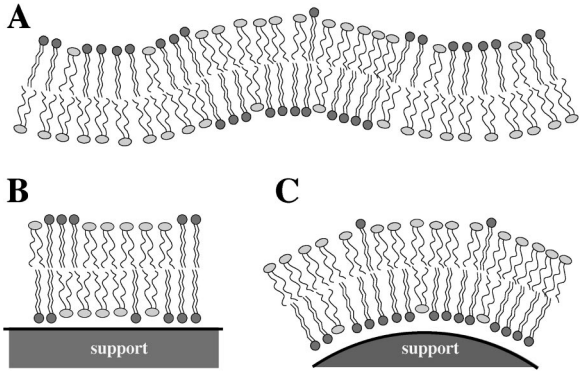

FIG. 6. Schematic drawing of an unsupported undulating membrane (A), a flat supported membrane (B), and a curved supported membrane (C). The unsupported membrane can freely adopt all available curvature states. The supported membranes in contrast are constrained in the ratio between the areas of the two monolayers.

We incorporate this constraint into the description by defining a curvature dependent harmonic potential G_{curv} which inhibits all bilayer states with a curvature different from $c_0 = 1/r_0$. For a flat membrane ($c_0 = 0$), this potential is be given by

$$G_{curv} = \alpha RTc(n_f^1, n_f^2)^2, \tag{3.14}$$

and for a curved membrane with two equivalent curvatures c_0 and $-c_0$ we define

$$G_{curv} = \alpha RT(c - c_0)^2 \tag{3.15}$$

or

$$G_{curv} = \alpha RT(c + c_0)^2. \tag{3.16}$$

The set of $[n_f^1, n_f^2]$ leading to a given curvature c is not necessarily unique. The constant α defines the strength of the curvature constraint. It is given a high value such that the fluctuations are constrained into a narrow interval around a given curvature. Using a potential of narrow width is necessary, because in a finite size matrix possible values for the curvature display discrete values. If a fixed curvature is chosen that does not correspond to one of these values, one has to sample around these values in a narrow interval. In our simulations α was chosen to be 10^5. However, the value of α does not influence the result as long as it is high enough to confine the fluctuations around a given curvature. Thus α is no simulation parameter.

The probability of finding a bilayer at a given point $(n_f^1, n_{gf}^1, n_f^2, n_{gf}^2)$ in phase space is given by

$$P_B(n_f^1, n_{gf}^1, n_f^2, n_{gf}^2, \zeta) = \frac{1}{Q_B} P_{M_1}(n_f^1, n_{gf}^1, \zeta) P_{M_2}(n_f^2, n_{gf}^2, \zeta) \times \exp\left(- \frac{G_{curv}(c)}{RT} \right), \tag{3.17}$$

where the monolayer partition coefficients P_{M_1} and P_{M_2} are identical to those defined in Eq. (3.6). The partition function of the curved bilayer, Q_B, normalizes the partition coefficients such that $\Sigma P_B = 1$.

Using constraints one can calculate the thermodynamic observables for lipid bilayers with different curvature (Fig. 7). Using the partition coefficients of Eq. (3.17), one can obtain the mean enthalpy $\langle H \rangle$ and the heat capacity c_p. In Fig. 7 the results for two different curvatures, $c = 0$ (flat membrane) and $1/c = r = 60$ nm, are given. The latter curvature approximately corresponds to large unilamellar vesicles. It can be seen that the heat capacity profile of the curved membrane (as compared to a flat membrane) is broadened and the c_P maximum is less pronounced. In the outer wings the heat capacity of the curved membrane is increased. The enthalpy change with temperature is broadened. Since curvature requires an asymmetry of gel and fluid lipids, even at very low temperatures the excess enthalpy does not approach zero (some fluid lipids remain on the outer monolayer). The same argument is equally true at high temperatures, where some gel lipids remain on the inner monolayer. The entropy of the system, either calculated from $S = -k\Sigma P_i \ln P_i$ or from integrating the heat capacity $[\Delta S = \int (c_P/T) dT]$ shows a similar temperature dependence. From both enthalpy and entropy profiles the Gibbs free energy G can be derived for the two curvatures. The free energy difference of the two curvature states, ΔG, corresponds to the elastic free energy necessary to bend the membrane (Fig. 7, bottom right panel). Obviously the free energy of bending displays a minimum at the melting temperature, in agreement with earlier theoretical considerations [15] and with experiments [30,31,25]. This means that the bending rigidity is largely decreased in the transition regime. At the heat capacity maximum of LUV's the bending modulus was found to be about five times smaller than in the fluid phase. Calculations of this kind were used in Ref. [26] to rationalize structural transitions in anionic lipid vesicles.

C. Lipid systems containing peptides

Let us now consider a lipid monolayer containing a small peptide similar in size to a lipid, e.g., an integral α-helical peptide. This problem can generally only be solved with a two-component Monte Carlo simulation. As in Eq. (3.4), the Gibbs free energy of a given configuration is

$$\Delta G(n_f, n_{gp}, n_{fp}, n_{gf}) = n_f(\Delta H - T\Delta S) + n_{gf}\omega_{gf} + n_{gp}\omega_{gp} + n_{fp}\omega_{fp}, \tag{3.18}$$

where ω_{gp} and ω_{fp} are contacts between the gel and peptide and the fluid and peptide, respectively. The histogram method presented here, however, allows us to calculate a special case of a lipid-peptide system, where the peptide resembles either the gel fluid lipid state. Peptides differ from gel lipids only in that peptides cannot melt. Such a case was considered in Ref. [10]. In the following let us assume that a peptide has similar properties to those of a gel lipid. This

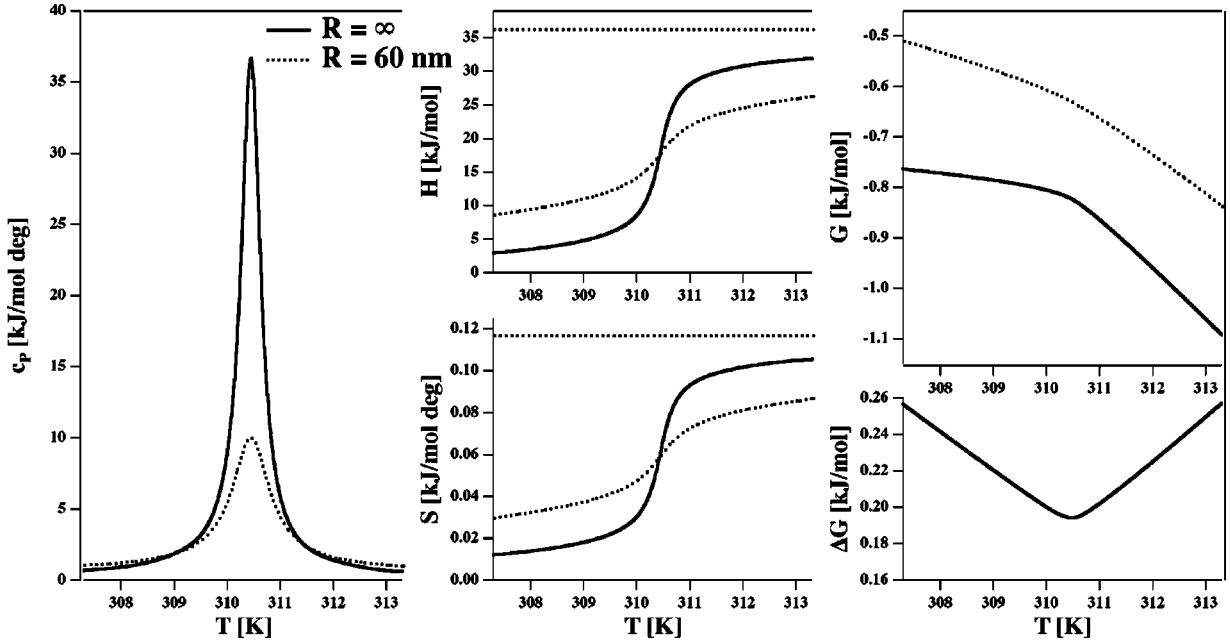

FIG. 7. Heat capacity, enthalpy, entropy and Gibbs free energy profiles for bilayers with two different mean curvatures, $c=0$ (solid lines) and $1/c=r=60$ nm (dotted lines), calculated by using a histogram as given in Eq. (3.17). Upon bilayer bending heat capacity profiles are broadened (left hand panel). Enthalpy and entropy of the membrane are significantly affected (center panels). The temperature dependence of the Gibbs free energy profiles are altered. The Gibbs free energy difference ΔG corresponds to the bending free energy . It displays a minimum at the melting temperature T_m (right hand panels). Simulation parameters were $\Delta H=36.4$ kJ/mol, $\Delta S=117$ J/mol deg, and $\omega_{gf}=1.3$ kJ/mol.

implies that the interfacial energy of a gel lipid with a peptide is similar to the contact between two gel lipids ($\omega_{gp}=0$), whereas a fluid lipid-peptide contact contributes to the overall Hamiltonian with $\omega_{fp}=\omega_{gf}$. This case is schematically shown in Fig. 8. It leads to a simplified expression for the Gibbs free energy for a given configuration of

$$\Delta G(n_f,n_{gf},n_{fp})=n_f(\Delta H-T\Delta S)+(n_{gf}^{fp})\omega_{gf}, \tag{3.19}$$

where $n_{gf}^{pf}=n_{gf}+n_{pf}$. With this expression the partition coefficients for this system can be derived from the lipid monolayer histogram,

$$P(n_f,n_{gf}^{fp},\zeta)=\frac{\Omega(n_f,n_{gf}^{fp},\zeta)\dfrac{(n_g+n_p)!}{n_g!n_p!}\exp\left(-\dfrac{\Delta G(n_f,n_{gf}^{fp},\zeta)}{RT}\right)}{\displaystyle\sum_{n_f}\sum_{n_{gf}}\Omega(n_f,n_{gf}^{fp},\zeta)\frac{(n_g+n_p)!}{n_g!n_p!}\exp\left(-\frac{\Delta G(n_f,n_{gf}^{fp},\zeta)}{RT}\right)}, \tag{3.20}$$

where $n_{gf}^{fp}=n_{gf}+n_{fp}$, and ζ is the set of parameter $[\Delta H,\Delta S,\omega_{gf},T]$. Equation (3.20) resembles Eq. (3.6) except for an additional combinatorial term, $(n_g+n_p)!/n_g!n_p!$, which accounts for the number of ways to arrange n_p gel-like peptides on the sites for gel and peptide in a given configuration. The heat capacities derived from this expression for different peptide concentrations n_p are given in Fig. 9. Depending on the peptide concentration, the c_P profiles are shifted to higher temperatures and are asymmetrically broadened, in agreement with Ref. [10]. For comparison, the results of a Monte Carlo simulation based on Eq. (3.18) are also given in Fig. 9 (solid symbols). They are in exact agreement with the solid line obtained from a histogram [Eq. (3.20)]. In the Monte Carlo simulation it can be seen that the asymmetry of the heat capacity profiles corresponds to an aggregation of the gel-like peptides in the fluid lipid membrane (cf. Ref. [10]) due to unfavorable fluid-peptide contacts.

IV. DISCUSSION

Using Monte Carlo simulations, we constructed a broad histogram for a lipid monolayer based on a two-state Doniach model [7]. We demonstrated how this histogram can be used to fit the experimental heat capacity profiles of different vesicular preparations of the zwitterionic lipid DPPC. Fur-

thermore, we used the monolayer histogram to calculate the behavior of lipid bilayers. This approach allows one to gain insight into many problems involving membrane bending that are not intuitive. We demonstrated that curvature leads to a broadening of the c_P profile, and that the free energy of the bending reaches a minimum at the melting temperature, in agreement with experimental results [30,31] and previous predictions [15]. We were also able to use the histogram method for a special case of membranes containing rigid peptides. Since the histogram contains the information for all relevant sets of parameters, it is possible to quasianalytically generate temperature profiles of the thermodynamic observables and the heat capacity.

Histogram reweighting methods to obtain thermodynamic observables as a continuous function of variables like temperature have been widely used. The technique was originally introduced in Ref. [29] and extended in Refs. [18,23]. Histograms can be obtained for a specific set of parameters, and used to calculate thermodynamic functions in the environment of the maximum of the original histogram. For a determination of the observables for a general set of parameters, one requires a broad histogram, covering most of the available phase space. This can be done by several methods: One can obtain the basic histogram at a critical point where fluctuations are large [19]. One can also combine many histograms obtained for different sets of parameters into one broad histogram by using reweighting and matching techniques [29,23,28]. An alternative approach, leading to broad histograms using a Monte Carlo method different from the Metropolis algorithm, was described in Refs. [32,33]. The multiple histogram method, proposed in Ref. [34], uses the dynamical ensemble [35]. In this paper we used a histogram technique as described in Ref. [18], and matched the histograms using a method similar to that introduced in Refs. [29,28]. Histogram methods have also been used to describe thermodynamic properties of membranes [20,14,4,36–38]. They were mainly applied to a ten-state Pink model or off-lattice Ising models [37,38]—systems that are too complex to obtain a universal broad histogram. The present paper is based on a two-state Doniach model [7]. Since it has only two variables, the number of fluid lipids and the number of contacts, one can create a two-dimensional broad histogram (Fig. 2).

Ising-like models have also been used previously to analyze lipid melting behavior [3,8,10,19,9,11]. In this paper we successfully used a broad histogram to fit the heat capacity profiles of various vesicular preparations of different mean curvature. This was done by varying the interfacial cooperativity parameter ω_{gf} with constant values for the melting enthalpy for a monolayer system, which is identical to assuming a bilayer with uncoupled monolayers. The outcome is that smaller systems with higher mean curvatures display a lower cooperativity. A lipid system with a lower melting cooperativity also possesses more pronounced wings of the c_P profile. A finite size scaling analysis indicated that fits to the c_P profiles of unilamellar vesicle preparations are independent of the matrix size. Multilamellar vesicles could only be described by limiting the maximum domain size or the size of the simulation matrix, respectively. This may be due to the finding that below the main chain melting transition a periodic ripple phase exists which has been proposed to limit domain sizes [11]. Thus the transition in MLV's resembles an all-or-nothing transition in a finite system of about 750 lipids. It could be well described by our histogram technique because the matrix size chosen by us is in this range (961 lipids). We were unable to describe it with a larger matrix using the Ising model. However, it cannot be excluded that due to the very narrow transition halfwidth heterogeneities in the sample (e.g., vesicular size variations) also play a role. It is unlikely that a more sophisticated model as the ten-state Pink model would yield better results. It has been found that the Pink model results in more pronounced wings of the transition profile [3]. In our experiments, however, pronounced wings are absent in the MLV profiles. An all-or-nothing transition, however, did not result in a reasonable description for LUV's and SUV's, which are not of first-order type.

Lipid bilayers consist of two monolayers. If the two monolayers are uncoupled they may freely fluctuate in local curvature. The curvature fluctuations are sometimes also referred to as undulations [39,40]. One conclusion from the present simulations was that curvature broadens the heat capacity profiles. This was also found experimentally in lipid membranes supported by latex beads of various curvature [27]. This suggests that the broadening of the experimental profiles in Fig. 4 may be partially caused by curvature. A fixed curvature acts as a reduction in cooperativity because fluctuations are hindered. In our model the number of lipids on both sides is kept constant. This assumption was used in an earlier paper [15] to predict the changes in curvature elasticity caused by fluctuations close to the melting transition. Recently these predictions were compared to experimental results on the membrane bending elasticity obtained using optical tweezers [25,41]. A perfect agreement between prediction and experimental result was found. We conclude, therefore, that our approach to fix the number of lipids on both sides is reasonable on typical experimental time scales. Of course these considerations require that the numbers of lipids on both monolayers are fixed. In the experimental systems shown in Fig. 4, the numbers of lipids on the outer and the inner monolayer may be different. In fact, curvature will result in a thermodynamic driving force that promotes an exchange between the inner and outer layers. At the c_P maximum the heat capacity is reduced as a consequence of the curvature. We concluded that the elasticity of curved supported membranes in the phase transition region is reduced as compared to a flat supported membrane. The curvature elasticity is related to fluctuations in the membrane curvature. Honger *et al.* [40] explained an unusual swelling of the multilamellar spacing of lipid vesicles close to the melting transition with curvature fluctuations. Fluctuations in the monolayer area have also been used to predict the temperature dependent reduction of the bending modulus close to the chain melting reaction [15], which were in agreement with experimental data based on flickering analysis of vesicular shapes [30,31]. Schneider *et al.* [26] argued that the experimentally observed change in elasticity must lead to a broadening of the heat capacity profiles, using an argument that is

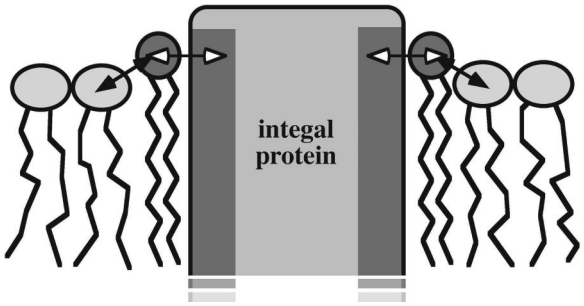

FIG. 8. Scheme of the nearest neighbor interactions in a lipid monolayer containing gel lipids, fluid lipids, and peptides. Shown are gel-fluid contacts and gel-peptide contacts.

just the reverse of the one presented here. In this paper, we calculated the free energy of bending from calculated heat capacity traces using the histogram method.

The decrease in bending rigidity gives rise to an enhanced probability of lipid vesicles undergoing structural changes close to the chain melting transition. The decrease of the elastic free energy necessary to bend membranes (as shown in Fig. 7) was used in Ref. [26] to explain structural transitions in charged lipid membranes. In these systems a change in vesicular morphology from vesicles to an extended bilayer network occurs close to the melting temperature. This work actually made use of some of the concepts outlined here. Another structural transition is the ripple phase formation. In most lipid systems one finds a small enthalpy transition below the main transition called a pretransition. It is linked to the formation of periodic membrane ripples. This transition was recently explained by the decrease in bending rigidity close to the chain melting transition [11], accompanied by the formation of a repeating pattern of gel and fluid lipid domains. It is likely that similar structural transitions occur frequently close to T_m.

Peptides and proteins have a pronounced effect on melting transitions. Usually lipid melting profiles are broadened and shifted, depending on the nature of the peptides and the lipids. It is believed that a significant source of the effect of the proteins originates from the ''hydrophobic matching'' [42]. If the length of the hydrophobic core of the protein is different from the lipid chain length, the interaction between the two components is unfavorable, and they do not mix well. In experimental studies where the lipid chain length was altered it could be seen that the effect of peptides on the melting reaction varies significantly [43]. The relevance of the hydrophobic matching condition was recently reviewed [44]. It was shown that there is considerable evidence of its importance for biological function. In the melting transition the thickness of bilayers decreases by about 16% [15]. Therefore, it is likely that the interaction of the proteins with the two lipid phases is not the same and that good mixing in one phase implies unfavorable mixing in the other state. The corresponding phase diagrams were discussed theoretically in Refs. [42,21,45]. Thus it is likely that proteins cluster or aggregate in one phase or the other. This change in protein distribution has pronounced effects on the melting behavior [10]. The c_P traces are shifted and asymmetrically broadened. From the shape of the melting curves one can in principle deduce how the components mix in either phase. For a suitable chain length of the lipids one can find proteins that mix well with one membrane state and do not mix with the other membrane state. Using the monolayer histogram technique we calculated the c_P curves for membranes containing peptides that mix well with the gel state and demix in the fluid state (Fig. 9). Depending on the peptide concentration, the curves are progressively shifted to higher temperatures and asymmetrically broadened with a shoulder at the high temperature end. Such a case was previously described theoretically in Refs. [42,10]. An experimental example for such a case is the mixing of the band-3 protein of erythrocytes with phosphatidylcholine membranes [46]. For a lipid chain length where the peptides mix well with the fluid phase, the situation is opposite: c_P profiles are shifted to lower temperatures with a shoulder on the low temperature site. This case can be treated equally well by exchanging n_{fp} with n_{gp} and n_g with n_f in Eq. (3.20). Experimental examples for such a case are given in Ref. [43].

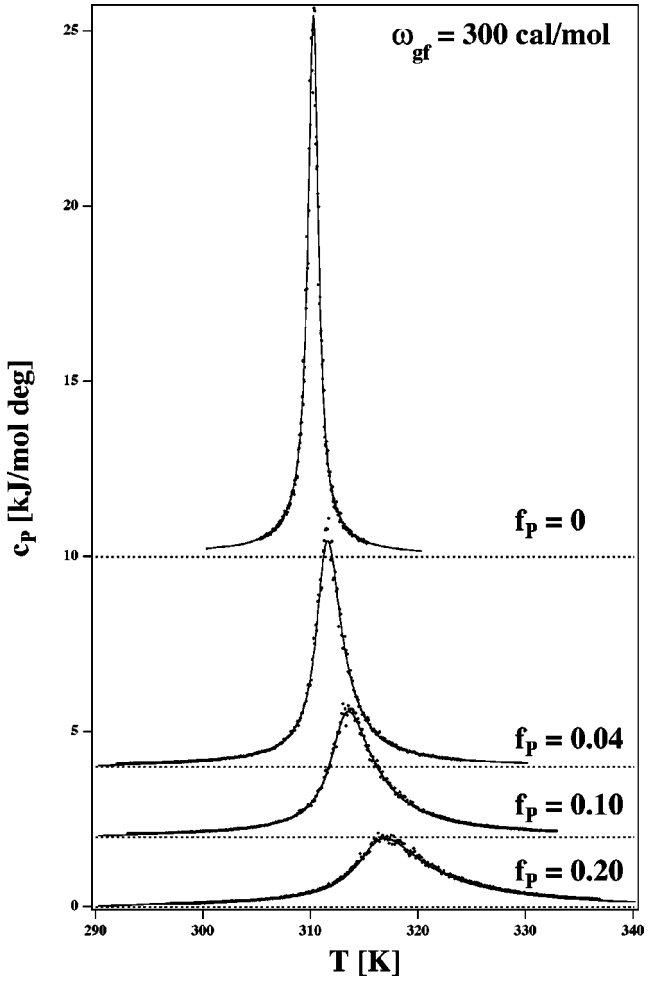

FIG. 9. Calculated heat capacity profile of a membrane containing various fractions of a gel-like peptide. Solid lines: calculated from Eq. (3.20). Small circles: calculated from a two component Monte Carlo simulation.

V. CONCLUSIONS

In this paper we described how a broad histogram method for lipid monolayers can be used to calculate properties of bilayers with different fixed curvatures, and simple systems containing peptides. We demonstrated that a simple model is able to rationalize properties of quite complex lipid systems. The main advantages of this approach are its simplicity and the fact that the histogram approach yields quasianalytical solutions for the general thermodynamic behavior of membranes.

ACKNOWLEDGMENTS

This work was supported by the Deutsche Forschungsgemeinschaft, Grant Nos. HE 1829/6-1 and HE 1829/8-1.

[1] S. Marcelja, J. Chem. Phys. **60**, 3599 (1974).
[2] S. Marcelja, Biochim. Biophys. Acta **367**, 165 (1974).
[3] O. G. Mouritsen *et al.*, J. Chem. Phys. **79**, 2027 (1983).
[4] J. Risbo, M. M. Sperotto, and O. G. Mouritsen, J. Chem. Phys. **103**, 3643 (1995).
[5] P. L. Hansen, L. Miao, and J. H. Ipsen, Phys. Rev. E **58**, 2311 (1998).
[6] O. G. Mouritsen, in *Molecular Description of Biological Membrane Components by Computer aided Conformational Analysis*, edited by R. Brasseur (CRC Press, Boca Raton, 1990), pp. 3–83.
[7] S. Doniach, J. Chem. Phys. **68**, 4912 (1978).
[8] I. P. Sugar, R. L. Biltonen, and N. Mitchard, in *Methods in Enzymology*, edited by L. Brand and M. L. Johnson (Academic Press, New York, 1994), Vol. 240, pp. 569–593.
[9] I. P. Sugar, T. E. Thompson, and R. L. Biltonen, Biophys. J. **76**, 2099 (1999).
[10] T. Heimburg and R. L. Biltonen, Biophys. J. **70**, 84 (1996).
[11] T. Heimburg, Biophys. J. **78**, 1154 (2000).
[12] I. P. Sugar and R. L. Biltonen, Methods Enzymol. **323**, 340 (2000).
[13] D. A. Pink and D. Chapman, Proc. Natl. Acad. Sci. U.S.A. **76**, 1542 (1979).
[14] E. Corvera, M. Laradji, and M. J. Zuckermann, Phys. Rev. E **47**, 696 (1993).
[15] T. Heimburg, Biochim. Biophys. Acta **1415**, 147 (1998).
[16] L. Cruzeiroe-Hansson, J. H. Ipsen, and O. G. Mouritsen, Biochim. Biophys. Acta **979**, 166 (1990).
[17] O. G. Mouritsen and K. Jorgensen, Mol. Membr. Biol. **12**, 15 (1995).
[18] A. M. Ferrenberg and R. H. Swendsen, Phys. Rev. Lett. **61**, 2635 (1988).
[19] T. Heimburg and D. Marsh, in *Biological Membranes: A Molecular Perspective from Computation and Experiment*, edited by K. M. Merz and B. Roux (Birkhäuser, Boston, 1996), pp. 405–462.
[20] Z. Zhang *et al.*, Phys. Rev. A **45**, 7560 (1992).
[21] Z. Zhang, M. M. Sperotto, M. J. Zuckermann, and O. G. Mouritsen, Biochim. Biophys. Acta **1147**, 154 (1993).
[22] G. Besold, J. Risbo, and O. G. Mouritsen, Comput. Mater. Sci. **15**, 311 (1999).
[23] A. M. Ferrenberg and R. H. Swendsen, Phys. Rev. Lett. **63**, 1195 (1989).
[24] E. A. Evans, Biophys. J. **14**, 923 (1974).
[25] R. Dimova, B. Pouligny, and C. Dietrich, Biophys. J. **79**, 340 (2000).
[26] M. F. Schneider *et al.*, Proc. Natl. Acad. Sci. U.S.A. **96**, 14312 (1999).
[27] T. Brumm, K. Jorgensen, O. G. Mouritsen, and T. M. Bayerl, Biophys. J. **70**, 1373 (1996).
[28] P. B. Bowen *et al.*, Phys. Rev. B **40**, 7439 (1989).
[29] J. P. Valleau and D. N. Card, J. Chem. Phys. **57**, 5457 (1972).
[30] L. Fernandez-Puente, I. Bivas, M. D. Mitov, and P. Meleard, Europhys. Lett. **28**, 181 (1994).
[31] P. Meleard *et al.*, Biophys. J. **72**, 2616 (1994).
[32] P. M. C. de Oliveira, T. J. P. Penna, and H. J. Hermann, Eur. Phys. J. B **1**, 205 (1998).
[33] J.-S. Wang, Eur. Phys. J. B **8**, 287 (1999).
[34] O. Hammrich, Z. Phys. B: Condens. Matter **92**, 501 (1993).
[35] R. W. Gerling and A. Hüller, Z. Phys. B: Condens. Matter **90**, 207 (1993).
[36] B. Dammann, H. C. Fogedby, J. H. Ipsen, and C. Jeppesen, J. Phys. I **4**, 1139 (1994).
[37] M. Nielsen *et al.*, Phys. Rev. E **54**, 6889 (1996).
[38] M. Nielsen *et al.*, Phys. Rev. E **59**, 5790 (1999).
[39] W. Helfrich, Z. Naturforsch. C **33**, 305 (1978).
[40] T. Honger *et al.*, Phys. Rev. Lett. **72**, 3911 (1994).
[41] T. Heimburg, Curr. Opin. Colloid Interface Sci. **5**, 224 (2000).
[42] O. G. Mouritsen and M. M. Sperotto, in *Thermodynamics of Cell Surface Receptors*, edited by M. Jackson (CRC Press, Boca Raton, FL, 1992), pp. 127–181.
[43] Y.-P. Zhang, R. N. A. H. Lewis, R. S. Hodges, and R. N. McElhaney, Biochemistry **34**, 2362 (1995).
[44] F. Dumas, M. C. Lebrun, and J. F. Tocanne, FEBS Lett. **458**, 271 (1999).
[45] O. G. Mouritsen *et al.*, in *Advances in Computational Biology*, edited by H. O. Villar (JAI Press, Greenwich, CT, 1995), pp. 15–64.
[46] M. R. Morrow, J. H. Davis, F. J. Sharom, and M. P. Lamb, Biochim. Biophys. Acta **858**, 13 (1986).